Intense High-Energy Proton Beams from Petawatt-Laser Irradiation of Solids

R. A. Snavely,[1,2] M. H. Key,[1] S. P. Hatchett,[1] T. E. Cowan,[1] M. Roth,[3,*] T. W. Phillips,[1] M. A. Stoyer,[1] E. A. Henry,[1] T. C. Sangster,[1] M. S. Singh,[1] S. C. Wilks,[1] A. MacKinnon,[1] A. Offenberger,[4,*] D. M. Pennington,[1] K. Yasuike,[5,*] A. B. Langdon,[1] B. F. Lasinski,[1] J. Johnson,[6] M. D. Perry,[1] and E. M. Campbell[1]

[1]*Lawrence Livermore National Laboratory, University of California, P.O. Box 808, Livermore, California 94550*
[2]*Department of Physics, University of California, Davis, Davis, California 95616*
[3]*GSI Laboratory, Darmstadt, Germany*
[4]*University of Alberta, Edmonton, Alberta, Canada T6G 2G7*
[5]*ILE, Osaka University, Suita, Osaka 565, Japan*
[6]*George C. Marshall Space Flight Center, Huntsville, Alabama 35812*

(Received 19 January 2000)

An intense collimated beam of high-energy protons is emitted normal to the rear surface of thin solid targets irradiated at 1 PW power and peak intensity 3×10^{20} W cm^{-2}. Up to 48 J (12%) of the laser energy is transferred to 2×10^{13} protons of energy >10 MeV. The energy spectrum exhibits a sharp high-energy cutoff as high as 58 MeV on the axis of the beam which decreases in energy with increasing off axis angle. Proton induced nuclear processes have been observed and used to characterize the beam.

PACS numbers: 41.75.Jv, 07.77.Ka, 52.50.Jm

The generation of fast protons from laser irradiated solid surfaces is well understood [1,2] and attributable to electrostatic fields produced by hot electrons acting on protons from adsorbed hydrocarbons. An empirical power law relationship between the mean proton energy and intensity x (wavelength) [2] ($I\lambda^2$) was identified and proton energies up to a few MeV were observed for $I\lambda^2$ up to 10^{18} W cm^{-2} μm^2 in nanosecond pulses [1]. Scaling laws for the maximum energy were similarly derived [3].

Chirped pulse amplification (CPA) laser technology [4] has since enabled widespread generation of terawatt power and the first petawatt laser [5]. CPA lasers generate pulses in the range 20 fs to 1 ps. 10 MeV protons were observed with a 1 ps CPA laser at $I\lambda^2 = 10^{19}$ W cm^2 μm^2 consistent with the previous scaling [6,7].

New mechanisms of ion acceleration have been studied with CPA lasers. Ponderomotive pressure of the laser radiation causes radial acceleration when laser beams are focused in gas jets and subcritical density plasmas [8] and also axial acceleration into solid targets [9]. Coulomb explosion of molecules [10] and clusters [11] has produced energetic ions. The ion energies from these newly studied processes have been <1 MeV/nucleon.

We report a laser induced proton beam with much higher particle energy (up to 58 MeV). The maximum energy is about $2\times$ higher than is given by extrapolating the previous scaling law [7] to the $30\times$ higher intensity of this work. A distinctive feature is emission with good beam collimation perpendicular to the rear-unirradiated surface(s) of the target. Similar rear surface beaming of protons of energy <1 MeV was reported in nanosecond pulse CO_2 laser experiments [12]. Our observed high proton energies open up access to nuclear processes.

The experiments used a CPA laser system generating 1 PW pulses of 500 fs duration [5]. With $f/3$ parabolic mirror focusing, the peak intensity was 3×10^{20} W cm^{-2} in a focal spot of 9 μm FWHM with 30% of the energy inside the first minimum. Amplified spontaneous emission in a 4 ns period before the main pulse had 10^{-4} of the main pulse energy and there was a 3×10^{-4} prepulse 2 ns before the main pulse. This precursor radiation generated a plasma which was measured by subpicosecond optical interferometry. The on axis electron density was 3×10^{19} cm^{-3} in a plane 70 μm from a flat CH polymer target with an approximately exponential fall to lower densities having a scale length of 40 μm [13].

The proton beam was recorded with radiochromic (RC) film which changes through polymerization of a diacetylene active layer, from transparent to dark blue in proportion to the dose (rads) of ionizing radiation (1 rad = 100 ergs/g). A 90° conical assembly of alternating Ta foils and sheets of RC film was used. The cone is 4 cm deep at its apex, which was placed 4.2 cm behind the target on the laser axis so the detector covered the forward hemisphere. The RC film response was calibrated absolutely and the image data were analyzed by digital densitometry and transformed geometrically to produce contour plots of dose as a function of angle illustrated in Fig. 1.

The data in Fig. 1 show a collimated intense proton beam emitted perpendicular to the rear target surface of a Au target at 45° to the laser axis. Its angular width narrows to 10° in the image through 600 μm of Ta. The beam is rather uniform in intensity with near circular sharp boundaries. There is a low intensity wide-angle background, which is discussed elsewhere and is due to escaping relativistic electrons [14]. Similar results were seen for normal incidence, S polarization, and target thickness down to 20 μm. The proton beam profiles from CH targets have nonuniform edges and exhibit internal fine structure as illustrated in Fig. 2 for a 100-μm thick CH target at normal incidence. There was typically a 5 times greater proton induced dose recorded from CH relative to Au targets. Data

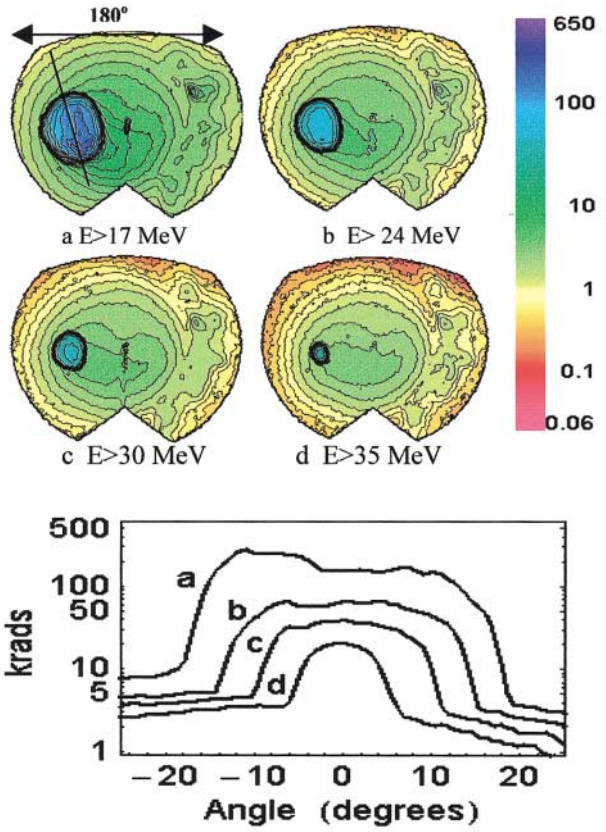

FIG. 1 (color). Top: Contour plots (a) to (d) of dose in kilorads (color bar units) as a function of angle after penetration through, respectively, 0.2, 0.4, 0.6, and 0.8 mm Ta in the detector. The target was a 1-mm square 125-μm thick Au foil irradiated with 465 J at 45° P polarized incidence. Bottom: Plot of beam profile lineouts showing krads as a function of angle in the vertical direction through the center of the proton beam along the path as indicated in (a).

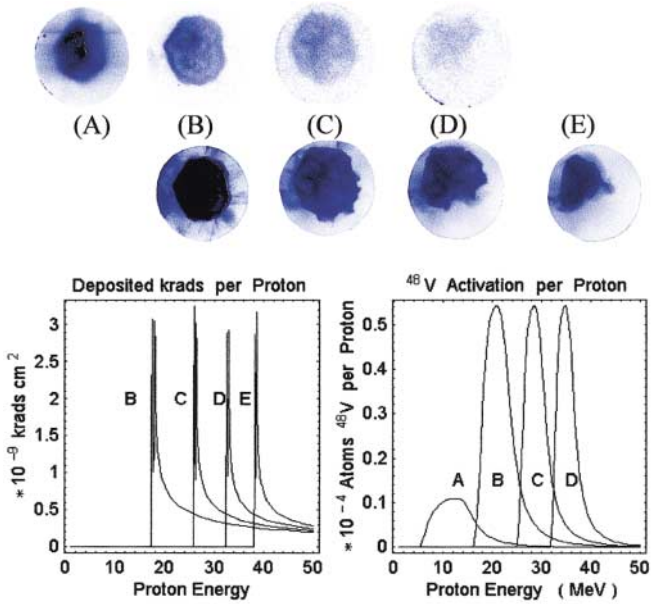

FIG. 2 (color). Data for a normal incidence 445 J shot on 100 μm CH from the Ti nuclear activation and RC film detector described later in the text: Ti foil autoradiographs (top row) and RC film images (middle row). The plots show Monte Carlo modeling of (below left) the RC film detector response in krads cm^2 per proton normally incident in the film layers; the nuclear activation response (below right) of the Ti layers to protons through the successive filter layers of the detector.

from more than 70 laser shots established that the angular characteristics were very reproducible and that the maximum energy was systematically related to laser intensity with some random variability. The proton identity of the beam was first suggested by analysis of etched tracks in CR39 plastic behind 7 mm of Al which gave evidence of $>$30 MeV protons.

The response of each RC film layer as a function of proton energy was calculated from stopping powers obtained with the SRIM code [15]. (An example for a similar detector package is shown in Fig. 2.) The integrated rad cm^2 in each image of the proton beam was determined from the RC film data. A deconvolution procedure was then used to relate these data to the film response (in rad cm^2 per proton) to give the absolute proton energy spectrum. Figure 3(a) shows an example in which the energy spectrum has a cutoff at about 58 MeV. We characterize the spectrum by fitting to an exponential with a mean energy of 4 MeV. The conversion fraction of laser energy to protons $E > 10$ MeV is 12% or 48 J. The extrapolation of the energy spectrum below 10 MeV is uncertain because the detector did not record protons of lower energy.

The sharp cutoff of the energy spectrum was also measured at 45° to the laser axis, via a hole in the RC film detector, using a magnetic spectrometer. These energy spectra were obtained from densitometry of photographic film as illustrated in Fig. 3(b) (below). For targets irradiated at 45° incidence the recorded spectrum was on the axis of the proton beam and in the example shown there is a cutoff at 55 MeV, while for normal incidence the recorded spectrum was at 45° off axis and the example shown has a cutoff at 15 MeV, consistent with the reduced cone angle for higher proton energies seen in Fig. 1. The photographic film is saturated so only the cutoff energies are significant in the plot. An estimate of the apparent source size of the proton emission (400 μm) was obtained from penumbral shadowing at the edge of the high energy end of the spectrum when a rectangular slit aperture was used and a 4 mm square 125-μm thick Au foil was irradiated [16].

Direct evidence that the beam is protons rather than other ion species was obtained from observation of nuclear reactions. A multilayer detector was used consisting of 3 cm diameter flat disks of 50 μm Ti, followed by three repeats of (1.2 mm Be, 250 μm Ti, and 250 μm RC film), then 1.5 mm Be and 250 μm RC film, placed 4.5 cm behind the target. The yield of the nuclear process, $^{48}\mathrm{Ti}(p,n)^{48}\mathrm{V}$ was measured absolutely from the characteristic gamma emission of the activated ^{48}V nuclei. The cross section has a threshold at 5 MeV and peaks at 13 MeV, 500 mbarn [17]. The activation was modeled using the stopping powers [15] and cross sections [17] to give the response of

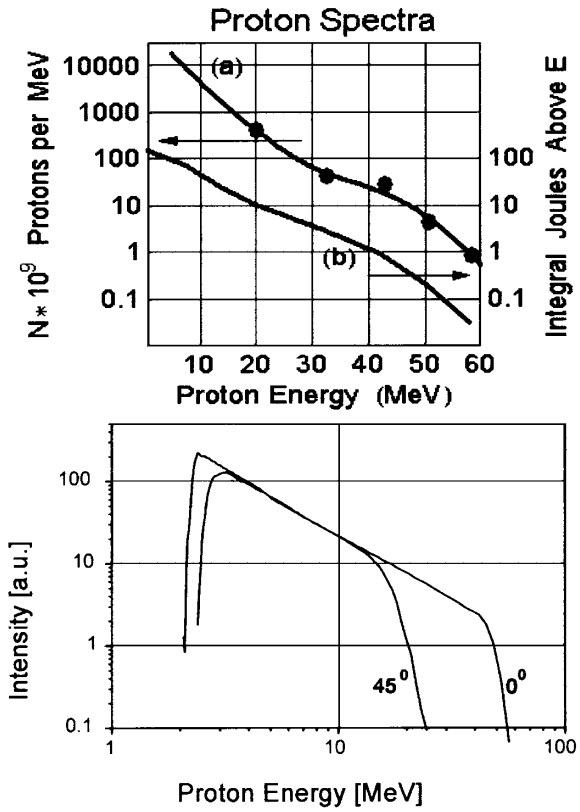

FIG. 3. (top) Proton energy spectrum deduced from radiochromic film images for a 423 J shot at normal incidence on 100 μm CH. (bottom) Spectrum of proton energy recorded on film with a magnetic deflection spectrometer. Plots show the spectrum on axis and from another shot at 45°. The detector is saturated above the cutoff region.

the detector in activations per proton in each Ti layer as in Fig. 2. A deconvolution procedure similar to that used for the RC film gave the absolute energy spectrum of the protons and close agreement was obtained comparing both methods.

In the example shown in Fig. 2 (445 J at normal incidence on 100 μm CH) there was an integrated energy of 30 J (3.5×10^{13} protons or 7% of the laser energy) in an exponential spectrum with a mean energy of 6 MeV. Autoradiographic images of the ^{48}V activation in the Ti foils (Fig. 2) clearly show a one to one correspondence to the RC film images recorded on the same shot from adjacent layers in the detector, giving further evidence that the RC film shows a proton beam. Another nuclear process observed was the production of 3×10^{10} neutrons on this shot (data from an Ag activation detector). This efficient yield (7×10^7 neutrons per joule) was from the several neutron producing channels of proton interaction with Be nuclei [18] and was an order of magnitude greater than neutron yields observed on shots without the Be disks.

Whether the beam was normal to the front or the rear surface of the target was assessed using a 2 mm wide 30° wedge target of CH as illustrated in Fig. 4. That the emission was normal to the rear surface is seen in the two separate proton beams in directions corresponding to

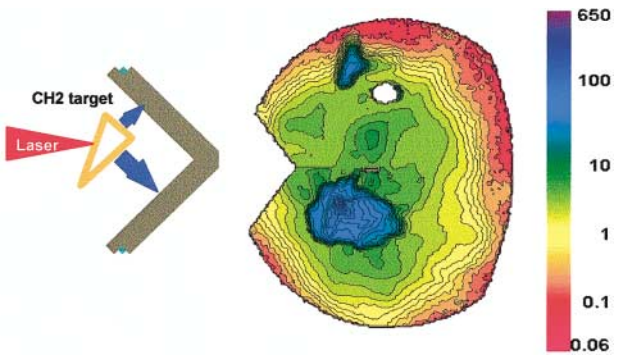

FIG. 4 (color). Contours of dose in krads as a function of angle recorded on a RC film through 300 μm Ta (proton $E >$ 18 MeV). The image clearly shows two proton beams, the larger from the major face and the smaller from the minor face of the wedge.

the normals to major and minor "rear" surfaces of the wedge.

RC images from 1-mm square thin foil targets through 25 μm Al (recording protons with energy >4 MeV) showed in addition to the intense beam, a weaker sheet of proton emission in the horizontal plane. We attribute this emission to the vertical edges of the target. This suggests that there is proton emission from an extended area of the rear surface of the target with lower energy protons emitted further from the center of the emitting surface.

Cones of radiochromic film placed both behind and (with a central hole for the laser beam) in front of a CH target for a target at 45° established that protons above the 12 MeV threshold energy for detection integrated over the forward hemisphere had less than 5% of the energy recorded in the proton beam from the rear surface.

We interpret the generation of the proton beam as a planar electrostatic acceleration by a dynamic Debye sheath formed at the rear target surface by hot electrons.

The focused main pulse generates an intense relativistic electron source. Relativistic self-focusing in the preformed plasma [19] enhances the intensity evidenced in our work by an invariant x-ray emission spot of ~20 μm diameter as the focal plane was displaced as much as 300 μm in front of the target [20]. We previously reported measurements of the energy spectrum of electrons, emitted from the rear surface of Au targets [21], showing electron energies up to 100 MeV and temperature of 5–10 MeV. The RC film data in Fig. 1 reveal the angular pattern of relativistic electron emission as a diffuse background. We determined the approximate source temperature and energy content of this electron emission by comparison of RC film exposure with Monte Carlo modeling. Typical results were 1–2 J of electrons and temperature of 3–4 MeV. The total emitted energy corresponds to the maximum charge which can leave the target before the Coulomb potential traps the major fraction of the electrons. The angular pattern of electron paths within the solid target is very broad. We observed a pattern of approximately 90°–180° FWHM for $E > 0.5$ MeV bremsstrahlung emitted from thick Au

targets. The measured total bremsstrahlung suggests that more than 40% of the laser energy is converted to relativistic electrons [14,22].

Identifying these electrons as the cause of the proton acceleration, we have adapted the standard model of fast ion generation by hot electrons [2] for very short pulse duration under the conditions of a preformed long scale length plasma on the front of the target and a short scale length at the unirradiated back surface.

A full discussion of the model is presented elsewhere [22,23]. Briefly, the electrons penetrate through the thin target ionizing H and other atoms at the rear surface where they set up a Debye sheath. Although the hot electron temperature T_h, the ion scale length L_i, and the hot electron Debye length L_d are dynamic, one can estimate the accelerating field from their initial values. Applying Poisson's equation and Boltzmann statistics for the electrons, the estimated initial accelerating field acting on the ions [24] is found to be $E = T_h/e \max(L_i, L_d)$ and normal to the rear surface. For example, if 40% of 500 J of laser energy were given to hot electrons of temperature $T_h = 6$ MeV which uniformly filled a volume of the target of dimensions of 300 μm diameter by 100 μm thickness (typical), then $L_d = 3.3$ μm and $E = 1.9$ MeV/μm. The power transfer to a proton would be >40 MeV/ps. There will be much stronger acceleration at the sharp density interface on the back of the target than on the front, where the preformed plasma scale length is very long as shown by our optical probe data discussed previously. Thus the rate of energy transfer to the ions is initially much greater on the back of the target where the acceleration process is dominated by the planar geometry phase of the plasma prior to significant expansion (in the example above, protons reach 40 MeV in 20 μm).

As the ions (plasma) expand, the acceleration rapidly drops because the expansion scale length enters the electric field formula above. The plasma develops a bell shaped radial structure due to the radial variation and the transverse spreading of the driving hot electrons within the target. The Debye sheath at the leading edge then develops a radial E field component off axis. Ions accelerated in these regions will reach lower energies with greater off axis angles (Fig. 1). 2D particle-in-cell simulations and semianalytic treatment have confirmed the applicability of this model and begin to quantify the observed relation between cutoff energy and angle.

We have concluded that light pressure effects at the front surface focal spot on the target could not generate the observed ions because of the clear evidence that the protons are emitted perpendicular to the rear surface(s) of the target. Observed proton emission from target edges supports a model of emission over an extended area much larger than the focal spot. Protons from Au targets could not come from the front surface focal region because the observed proton flux exceeds that available from adsorbed monolayers in the focal region and the prepulse would have cleaned the surface in any event.

Proton beams of the high energy, power, and collimation observed here could be of interest for numerous applications, from medical ion beam cancer therapy to the production of short-lived radionuclides. Characterization of the emittance will determine the focusability of the beam and its usefulness, for example, in replacing the front end of large accelerators or as an ignitor in fast ignition. The ion acceleration process is not restricted to protons. With preparation, massive ions could be accelerated to similar energy per nucleon.

We are grateful to C. Brown for his operation of the Petawatt Laser System. This work was performed under the auspices of the U.S. Department of Energy by the Lawrence Livermore National Laboratory under Contract No. W-7405-ENG-48.

Note added.—We are aware of the more recent work [25] arguing for front surface ion acceleration in contrast to our rear surface ion acceleration observations, theory, and modeling.

*Visitor.

[1] S. J. Gitomer *et al.,* Phys. Fluids **29**, 2679 (1986).
[2] Y. Kishimoto *et al.,* Phys. Fluids **26**, 2308 (1983).
[3] H. Tan *et al.,* Phys. Fluids **27**, 296 (1984).
[4] M. D. Perry and G. Morou, Science **264**, 917 (1994).
[5] M. D. Perry *et al.,* Opt. Lett. **24**, 160 (1999).
[6] A. P. Fews *et al.,* Phys. Rev. Lett. **73**, 1801 (1994).
[7] F. N. Beg *et al.,* Phys. Plasmas **4**, 447 (1997).
[8] G. Pretzler *et al.,* Phys. Rev. E **58**, 1165 (1998).
[9] M. Zepf *et al.,* Phys. Plasmas **3**, 3242 (1996).
[10] K. Codling and L. J. Frazinski, Contemp. Phys. **35**, 243 (1994).
[11] T. Ditmire *et al.,* Nature (London) **398**, 489 (1999).
[12] D. M. Villeneuve *et al.,* Phys. Rev. A **27**, 2656 (1983).
[13] A. J. MacKinnon *et al.,* Bull. Am. Phys. Soc. **44**, 7 (1999).
[14] M. H. Key *et al.,* in *Proceedings of the 1st International Conference on Inertial Fusion Sciences and Applications, Bordeaux, France, 1999* (Elsevier, Paris, 2000).
[15] J. F. Ziegler, J. P. Biersack, and U. Littmark, *The Stopping and Range of Ions in Solids* (Pergamon Press, New York, 1996).
[16] T. E. Cowan *et al.* (to be published).
[17] H. I. West, Jr., R. G. Lanier, and M. G. Mustafa, Lawrence Livermore National Laboratory, Livermore, CA, Report No. UCRL-ID-115738, 1993.
[18] J. K. Blair, C. M. Jones, and H. B. Willard, Nucl. Phys. **53**, 209 (1964).
[19] A. Pukhov and J. Meyer ter Vehn, Phys. Rev. Lett. **76**, 3975 (1996).
[20] M. H. Key *et al.,* in *Proceedings of the 17th IAEA Fusion Energy Conference 98* (International Atomic Energy Agency, Vienna, 1999), Vol. 3, p. 1093.
[21] T. Cowan *et al.,* Phys. Rev. Lett. **84**, 903 (2000).
[22] S. Hatchett *et al.,* Phys. Plasmas **7**, 5 (2000); **7**, 2078 (2000).
[23] S. Wilks *et al.* (to be published).
[24] J. Denavit, Phys. Fluids **22**, 1384 (1979).
[25] E. L. Clark *et al.,* Phys. Rev. Lett. **84**, 670 (2000); A. Maksimchuk *et al.,* Phys. Rev. Lett. **84**, 4108 (2000).